Incorporation of Triacylglycerol and Cholesteryl Ester Droplets in Phase-Separated Giant Unilamellar Vesicles

Chiho Kataoka-Hamai,[1,]* *Jingwen Song,*[1] *and Kohsaku Kawakami*[1,2]

[1]Research Center for Macromolecules and Biomaterials, National Institute for Materials Science, 1-1 Namiki, Tsukuba, Ibaraki 305-0044, Japan

[2]Graduate School of Pure and Applied Sciences, University of Tsukuba, 1-1-1 Tennodai, Tsukuba, Ibaraki 305-8577, Japan

ABSTRACT Cytoplasmic lipid droplets form from the endoplasmic reticulum. Because the endoplasmic reticulum membrane can undergo phase separation, the interaction of lipid droplets with phase-separated bilayers is of significant interest. In this study, we used fluorescence microscopy to investigate the incorporation of droplets composed of triolein, trilinolein, trimyristolein, trieicosenoin, and cholesteryl arachidonate in the bilayers of giant unilamellar vesicles (GUVs) consisting of a mixture of 1,2-dioleoyl-*sn*-glycero-3-phosphocholine (DOPC), 1,2-dipalmitoyl-*sn*-glycero-3-phosphocholine (DPPC), and cholesterol. After incorporating the triacylglycerol droplets, the DOPC/DPPC/cholesterol (3:3:2) GUVs, which exhibited liquid-disordered (L_d) and liquid-ordered (L_o) phase separation, retained their phase-separated state. The triacylglycerol droplets predominantly partitioned in the L_d domains. To elucidate the basis of this preferential partitioning, we investigated the surface pressures of DOPC, DPPC, and cholesterol monolayers containing triolein at the air–water interface using a Langmuir trough. From these measurements, we determined the interfacial tension at the monolayer-covered triolein–water interface. The results showed that DOPC most effectively reduced the interfacial tension. Thus, the droplet sorting into the DOPC-enriched L_d domains likely arose from the difference in the abilities of the two phases to stabilize the droplet interface. In contrast, cholesteryl arachidonate had a profound effect on the bilayer phase behavior. Fluorescence images of the DOPC/DPPC/cholesterol (3:3:2) GUVs showed that the domain structures disappeared after droplet incorporation. Additionally, surface pressure measurements of DOPC/DPPC/cholesterol (3:3:2) monolayers containing cholesteryl arachidonate at the air–water interface suggested that cholesteryl arachidonate weakened the lipid–lipid interaction. The results indicate that the cholesteryl arachidonate molecules diffused across the bilayer to hinder bilayer phase separation.

INTRODUCTION

Neutral lipids are stored in cytoplasmic lipid droplets. In eukaryotes, the lipid droplets consist of a neutral lipid core surrounded by a phospholipid monolayer decorated with proteins.[1, 2] The main components of the hydrophobic core are triacylglycerols (TAGs) and sterol esters (SEs). Lipid droplets emerge from the endoplasmic reticulum (ER).[1-3] Neutral lipids are first synthesized and dispersed within the ER membrane. As their concentration increases, the neutral lipids aggregate to form a lens-like structure between the monolayer leaflets. This lens-like structure subsequently grows into a droplet, which eventually buds off from the ER membrane. These processes are regulated by various proteins.[4, 5]

To better understand lipid droplet biogenesis, it is first necessary to understand the characteristics of droplet-incorporating bilayers in the absence of proteins. Model membrane systems are useful for such investigations. Previous studies have used model systems such as giant unilamellar vesicles (GUV),[6-8] supported lipid bilayers,[9, 10] multilamellar lipid films,[11] free-standing bilayers,[12] and droplet interface bilayers.[13] These studies have provided several important insights. First, the TAG droplets in a bilayer grow or shrink via Ostwald ripening, where TAG molecules diffuse from small to large droplets through the bilayer.[9, 10] Second, the budding direction of the droplets is determined by the membrane tension of the monolayer leaflets, and a droplet buds toward the leaflet with lower monolayer tension.[6] Third, incorporating free TAG molecules in curved bilayers is energetically disfavored compared with incorporation in flat bilayers, whereas free SE molecules readily incorporate in curved bilayers.[8] Moreover, TAG droplets induce bilayer spontaneous curvature, which can influence the overall vesicle structure.[7] These previous studies used one- or two-component bilayers in a single fluid phase, labeled with a low concentration of a fluorescent probe lipid. The ER membrane was once thought to form a uniform, fluid bilayer because of its low cholesterol content.[14, 15] However, recent studies have shown that the ER membrane can phase-separate into fluid and gel-like phases,[16-18] and the gel-like domains localize at the ER–lipid droplet contact sites.[16] Thus, it is interesting to investigate the interactions between lipid droplets and phase-separated bilayers.

In this study, we investigated the incorporation of isotropic liquid droplets of TAGs and SE in bilayers consisting of liquid-disordered (L_d) and liquid-ordered (L_o) phases. To mimic the phase separation in the ER, it is desirable to use a bilayer consisting of L_d and gel (solid-ordered (S_o)) phases. However, it is not easy to obtain such bilayer systems. Although binary mixtures of saturated and unsaturated phospholipids are known to exhibit the L_d–S_o phase transition, their phase behavior is complex, involving the formation of L_d, S_o, sub-gel, and ripple phases.[19-23] Thus, to simplify the experimental system, we used a bilayer composed of L_d and L_o phases instead of L_d and S_o phases. The L_d, L_o, and S_o phases differ in their fluidity. The lipid diffusion coefficients in L_o and S_o phases are typically 10^2 and 10^5 times smaller than those in L_d phases, respectively.[24] The cholesterol concentrations in the L_o and S_o phases are also different, although they are similar with a high content of saturated phospholipids.[23, 25] Thus, the membrane systems investigated in this study are not relevant to the biological system. However, it is still interesting to understand the interaction of a droplet with the two domains with different fluidities.

TAGs generally form crystals at low temperatures and transition to isotropic liquids at higher temperatures. In this study, we investigated four TAGs—triolein, trilinolein, trimyristolein, and trieicosenoin (Figure 1)—all of which are isotropic liquids at room temperature. Triolein and trilinolein are present in lipid droplets in plant and mammalian cells.[26-28] For the SE, we investigated cholesteryl arachidonate (Figure 1). Most SEs are crystals at room temperature and form various types of liquid crystals after heating.[29] However, unlike typical SEs, cholesteryl arachidonate does not form any mesophases and is an isotropic liquid at room temperature.[29] Thus, we chose cholesteryl arachidonate to focus on the behavior of the liquid droplets. Cholesteryl arachidonate is present in lipid droplets in mammalian cells.[30-32]

Here, we investigated the incorporation of droplets consisting of triolein, trilinolein, trimyristolein, trieicosenoin, and cholesteryl arachidonate in DOPC/DPPC/cholesterol (3:3:2) GUVs. We show that TAG droplets preferentially partition in L_d phase domains, whereas cholesteryl arachidonate droplets disrupt bilayer phase separation.

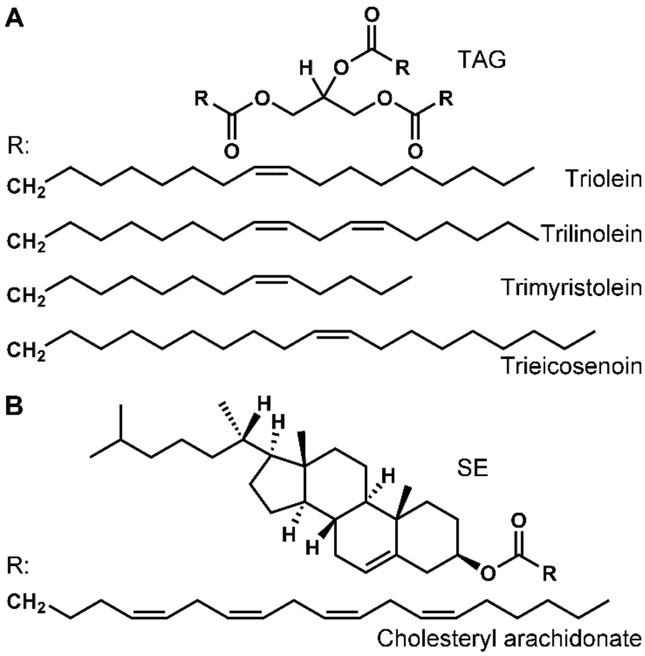

FIGURE 1. Chemical structures of the (A) triacylglycerols (TGAs) and (B) sterol ester (SE) used in this study.

Experimental Section

Materials. 1,2-Dioleoyl-*sn*-glycero-3-phosphocholine (DOPC) and 1,2-dipalmitoyl-*sn*-glycero-3-phosphocholine (DPPC) were purchased from Avanti Polar Lipids (Alabaster, AL, USA). The concentrations of the phospholipid stock solutions in chloroform were determined by phosphorus assay.[33] Cholesterol and cholesteryl arachidonate were purchased from Nu-Check Prep (Elysian, MN, USA). The concentrations of the cholesterol and cholesteryl arachidonate stock solutions in chloroform were determined by a colorimetric assay kit (FUJIFILM Wako Pure Chemical Corporation, Osaka, Japan). Triolein, trilinolein, trimyristolein, and trieicosenoin were purchased from Nu-Check Prep. The fluorescent probes 1,2-dipalmitoyl-*sn*-glycero-3-phosphoethanolamine-*N*-(7-nitro-2-1,3-benzoxadiazol-4-yl) (ammonium salt) (NBD-DPPE) and 1,2-dioleoyl-3-[11-(dipyrrometheneboron difluoride)undecanoyl]-*sn*-glycerol (TopFluor-TG) were purchased from Avanti Polar Lipids. Texas Red 1,2-dihexadecanoyl-*sn*-glycero-3-phosphoethanolamine, triethylammonium salt (TR-DHPE) and 4,4-difluoro-1,3,5,7,8-pentamethyl-4-bora-3a,4a-diaza-*s*-indacene (BODIPY 493/503) were purchased from Thermo Fisher Scientific (Waltham, MA, USA). The glass coverslips (25 mm diameter, no.1) were purchased from Matsunami Glass Ind., Ltd. (Osaka, Japan).

GUV Preparation. The GUVs were prepared by electroformation as follows.[34-36] The lipids were mixed with a desired lipid composition in chloroform to yield a concentration of 3.5 mM. The lipid solution (4 μL) was spread onto two platinum electrodes (0.5 mm diameter) separated by ~1 mm. After the evaporation of chloroform under a nitrogen stream, the electrodes were immersed in 300 mM sucrose (200 μL) incubated at 55 °C, followed by the application of alternating sign-wave signals with a peak-to-peak amplitude of 2.2 V for 35 min. The frequencies for the first 30 min and final 5 min were 10 and 2 Hz, respectively. For the investigation of the bilayer phases in the GUVs before droplet incorporation, the GUV samples were cooled from 55 to 25 °C at a rate of 0.1 °C/s using a thermal cycler (MyCycler, Bio-Rad, Hercules, CA, USA). For the investigation of the GUVs with oil droplets, the temperature of the GUV samples was maintained at 55 °C for the subsequent droplet incorporation process. The lipid compositions of the GUVs are expressed as molar ratios.

Droplet Incorporation in the GUVs. The TAGs and cholesteryl arachidonate were mixed with TopFluor-TG (0.005 mol %) and BODIPY 493/503 (0.005 mol %), respectively. The dye-labeled oil sample (0.3 µL) was suspended in an aqueous solution (30 µL) containing 40 mM NaCl, 191 mM sucrose, and 10 mM NaH_2PO_4–Na_2HPO_4 (pH 7.4). The addition of sodium chloride is necessary to promote droplet incorporation.[7] The sucrose concentration was adjusted so that the osmotic pressure across the bilayers did not significantly change during the following droplet incorporation process. The oil suspension was subsequently sonicated for 10 min in an ultrasonic bath, vortexed, and further sonicated for 10 min. The temperature of the sonication bath water was in the range 20–31 °C. Immediately after sonication, the emulsion sample (7.5 µL) was added to a GUV sample (0.07 mM lipid, 7.5 µL) pre-incubated at 55 °C. To enhance the droplet incorporation efficiency, the samples were heated above the phase transition temperature of DPPC (41 °C).[37] The sample was slowly mixed by pipetting four times, followed by incubation at 55 °C for 30 min in the dark. The sample was mixed by tapping every 5 min during incubation. The sample was finally cooled from 55 to 25 °C at a rate of 0.1 °C/s using the thermal cycler (MyCycler, Bio-Rad).

Sample Preparation for Fluorescence Imaging. The glass coverslips were cleaned with ethanol and dried in a nitrogen stream before use. For fluorescence imaging of the oil-free GUVs, the GUV samples (50 µL) were diluted with 300 mM glucose (450 µL), followed by deposition onto a glass coverslip in an Attofluor cell chamber (Thermo Fisher Scientific). For fluorescence imaging of the GUVs with oil droplets, the samples (15 μL) were diluted in 300 mM glucose (60 μL) and deposited onto a glass coverslip in a poly(dimethylsiloxane) chamber. The coverslip was fixed in an Attofluor cell chamber. The glucose solution was used to sediment GUVs near the glass surface. For fluorescence imaging of the planar bilayer patches, the glass coverslips pre-cleaned in ethanol were exposed to air plasma generated with a PDC-32G plasma cleaner (Harrick Plasma, Ithaca, NY, USA) for 2 min immediately before use. The GUV samples (40 μL) were diluted with an aqueous solution containing 44 mM sodium chloride and 287 mM glucose (360 μL), followed by adsorption on the plasma-cleaned glass coverslips for 15 min in Attofluor cell chambers. The glass surfaces were subsequently washed with 40 mM NaCl to remove unbound vesicles.

Confocal Laser Scanning Microscopy. The confocal fluorescence imaging was performed with a Zeiss LSM 900 microscope (Carl Zeiss, Oberkochen, Germany) at a magnification of 63×. TR-DHPE was excited with a 561-nm laser. NBD-DPPE, TopFluor-TG, and BPDIPY 493/503 were excited with a 488-nm laser. Two GaAsP detectors were used in confocal imaging mode. An Airyscan 2 imaging device was used in super-resolution imaging mode. The data acquisition and deconvolution were performed with ZEN (blue edition) software (version 3.4.91.00000, Carl Zeiss).

Epifluorescence Microscopy. The epifluorescence imaging was performed with an Eclipse Ti-E microscope (Nikon, Tokyo, Japan) equipped with an electron-multiplying charge-coupled device camera (iXon EM + 897E, Andor Technology, Belfast, UK). The samples were imaged at magnifications of 40× and 100× under light-emitting-diode (LED) illumination (X-Cite Xylis

XT720L, Excelitas Technologies Corp., Pittsburgh, PA, USA). The filter sets used for TR-DHPE and NBD-DPPE were FF01-561/12:Di01-R561:FF01 609/54 and FF01-482/18:Di01-R488:FF01-525/45, respectively (Semrock, IDEX Health & Science, Oak Harbor, WA, USA).

Surface Pressure Measurements at the Air–Water Interface and Langmuir–Blodgett Monolayer Transfer. The surface pressure measurements and monolayer transfer were performed using a Langmuir trough with a size of 35 cm × 7.5 cm (KSV NIMA, Biolin Scientific, Gothenburg, Sweden). A lipid mixture in chloroform (~1 mM) was spread onto a pure water surface in the trough. The compositions of the lipid mixtures are expressed as molar ratios. The subphase water temperature was kept constant at 23 °C using a water circulator. After allowing the solvent to evaporate for 2 min, the monolayer was compressed at a rate of 15 mm/min by two barriers. The surface pressure was recorded using a platinum Wilhelmy plate with a perimeter of 20 mm. For monolayer transfer onto the surface of muscovite mica (grade v-4, Structure Probe, Inc., West Chester, PA, USA), a DPPC/triolein (4:1) film was compressed until the surface pressure reached 35 mN/m. After equilibration for 4 min, the monolayer was transferred onto a freshly cleaved mica surface by withdrawing the substrate (8.5 mm × 25 mm) from the subphase water at a rate of 5 mm/min.

Pendant Drop Tensiometry. The interfacial tension at the pure triolein–water interface was measured at room temperature (23 °C) using a DSA drop shape analyzer (Krüss GmbH, Hamburg, Germany). A j-shaped needle attached to a glass syringe was first immersed in water. A triolein drop (density 0.91 g/mL)[38, 39] was then formed at the needle end by dispensing triolein from the syringe. The drop shape was recorded under LED illumination, and it was fitted to the Young–Laplace equation using ADVANCE software (Krüss GmbH). The interfacial tension of the triolein–water interface was determined to be 30.9 (±0.1) mN/m ($N = 3$), which is consistent with previously reported values.[40, 41]

Atomic Force Microscopy. The atomic force microscopy (AFM) imaging was performed in dynamic mode with an SPI4000/SPA400 system (SII NanoTechnology, Tokyo, Japan). A cantilever with a force constant of ~42 N/m and a resonance frequency of ~300 kHz (OMCL-AC-160TS, Olympus, Tokyo, Japan) was used.

Experimental Values. The reported values are the mean values (±standard error) of N determinations.

Results and Discussion

Phase Separation in Droplet-Free Bilayers. We used DOPC/DPPC/cholesterol (3:3:2) GUVs labeled with 0.1% TR-DHPE and 0.2% NBD-DPPE and DOPC/DPPC/cholesterol (1:12:7) GUVs labeled with 0.3% NBD-DPPE for droplet incorporation. A previous study reported that the DOPC/DPPC/cholesterol (3:3:2) mixture consists of L_d and L_o phases, while the DOPC/DPPC/cholesterol (1:12:7) mixture forms a single L_o phase.[42] However, trace amounts of fluorescent probes can alter the bilayer phase diagrams.[43] Therefore, we first confirmed the phase states of the GUVs by epifluorescence microscopy (Figure 2). The DOPC/DPPC/cholesterol (3:3:2) GUVs exhibited fluorescence patterns characteristic of phase separation. In the TR fluorescence images (Figure 2A), the bright and dark domains were assigned to the L_d and L_o phases, respectively, because TR-DHPE predominantly partitions in L_d domains.[44] We also observed planar bilayer patches on the glass surface formed by GUV rupture (Figure 2B and C).[35]

The TR and NBD fluorescence images had opposite contrasts, which is consistent with previous observations that NBD-DPPE favors L_o domains.[45] The fluorescence images of the planar bilayer patches sometimes exhibited a circular pattern characterized by TR and NBD fluorescence signals with opposite contrasts (Figure 2B and C). These patterns are expected to arise from the domain redistribution occurring in the deformed vesicles before rupture, as previously reported.[35] Using the fluorescence images of the planar bilayer patches, we determined the surface area ratio of the L_d phase to be 61.7% (±1.1%, $N = 60$).

The DOPC/DPPC/cholesterol (1:12:7) GUVs showed homogeneous NBD fluorescence signals for both vesicles (Figure 2D) and planar bilayer patches (Figure 2E). Thus, the single L_o phase formed.

For droplet incorporation, we used DOPC/DPPC/cholesterol (3:3:2) GUVs labeled with TR-DHPE and NBD-DPPE as the phase-separated bilayer and DOPC/DPPC/cholesterol (1:12:7) GUVs labeled with NBD-DPPE as the L_o-phase bilayer. TR-DHPE and NBD-DPPE were used to visualize the L_d and L_o phases, respectively.

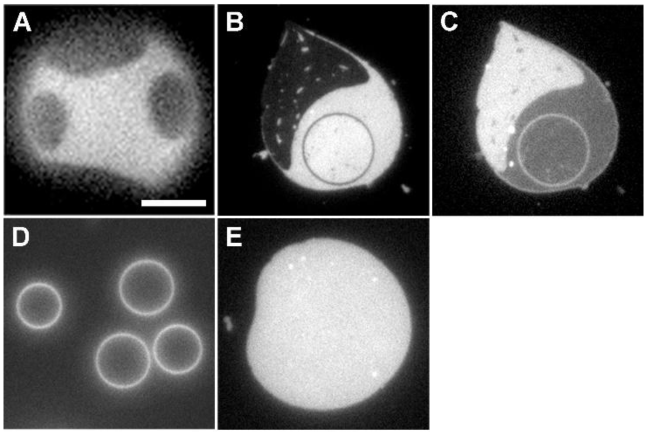

FIGURE 2. Epi-fluorescence images of the (A)–(C) DOPC/DPPC/cholesterol (3:3:2) bilayers and (D) and (E) DOPC/DPPC/cholesterol (1:12:7) bilayers. (A) TR fluorescence image of a

GUV near the glass surface. (B) TR and (C) NBD fluorescence images of a planar bilayer patch on glass. NBD fluorescence images of (D) free vesicles and (E) a planar bilayer patch on glass. The scale bar in (A) is 10 μm. All of the images are on the same scale. The magnification was 40× for (A) and 100× for (B)–(E).

Incorporation of TAG Droplets in the GUVs. We investigated the incorporation of TAG droplets in the DOPC/DPPC/cholesterol (3:3:2) GUVs by confocal microscopy. The droplets were labeled with TopFluor-TG. The fluorescence signals from NBD-DPPE and TopFluor-TG were recorded through the same acquisition channel (Figure 3A–C, panels i (green) and iii), whereas those from TR-DHPE were collected through another channel (panels i (magenta) and ii). The images showed that most of the droplets existed in L_d domains. Among these droplets, some were incorporated in the inter-leaflet space in the bilayers (Figure 3A), while others were bound to the outer vesicle surface exposed to the external solution (Figure 3B). Additionally, a few droplets were attached to the outer vesicle surface in the L_o phase (Figure 3C). However, the monolayers of these droplets showed higher TR fluorescence intensities than the L_o-phase bilayers (Figure 3C, panel ii). Because TR-DHPE partitions in loosely packed membranes, the droplets on the L_o phase were likely covered with a more loosely packed monolayer than the L_o phase. The statistics (Figure 3D) showed that all of the triolein and trilinolein droplets were in the L_d phase: ~80% were incorporated near the bilayer center (Figure 3D, gray bar), as in Figure 3A, while the remaining ~20% of the droplets were bound to the outer vesicle surface (Figure 3D, black bar), as in Figure 3B. For trimyristolein and trieicosenoin, ~20%–30% of the droplets were bound to the outer vesicle surface in the L_o phase (Figure 3D, white bar), as in Figure 3C. The reason why this binding only occurred for trimyristolein and trieicosenoin is unclear. However, similar to the results for triolein and trilinolein, all of the other droplets were embedded in the inter-leaflet space in the L_d phase (Figure 3D, gray bar), as in Figure 3A.

In a previous study, we found that TAG droplets were easily incorporated in DOPC GUVs.[7] In the present study, the L_d phase had a high DOPC ratio, whereas the L_o phase had high DPPC and cholesterol ratios.[42] Thus, the present results may indicate that the TAG droplets were unable to penetrate the DPPC- and cholesterol-rich bilayers. To investigate this possibility, we incorporated triolein droplets in the DOPC/DPPC/cholesterol (1:12:7) GUVs in a uniform L_o phase. According to a tie line in a reported phase diagram,[42] the L_o phase in DOPC/DPPC/cholesterol (3:3:2) has a lipid ratio of 5:12:8. Thus, the DOPC/DPPC/cholesterol (1:12:7) mixture contained higher DPPC and cholesterol concentrations than the L_o phase in the DOPC/DPPC/cholesterol (3:3:2) mixture. The fluorescence images of the DOPC/DPPC/cholesterol (1:12:7) GUVs showed successful incorporation of triolein droplets (Figure 3E). Therefore, DPPC and cholesterol were unlikely to preclude the inclusion of droplets. Thus, we expected that the droplets were sorted into the L_d domains owing to the energetic balance between the incorporation in the L_d phase and that in the L_o phase.

In a previous study using phosphatidylcholine (PC) GUVs in uniform fluid phases, we found that the exposure to TAG droplets results in two main membrane structures: a unilamellar vesicle with droplets and a vesicle with droplets consisting of a single-bilayer spherical segment and a double-bilayer spherical segment.[7] Consistent with this previous study, we observed vesicles composed of single- and double-bilayer regions (Figure S1). However, we did not analyze these two-region vesicles.

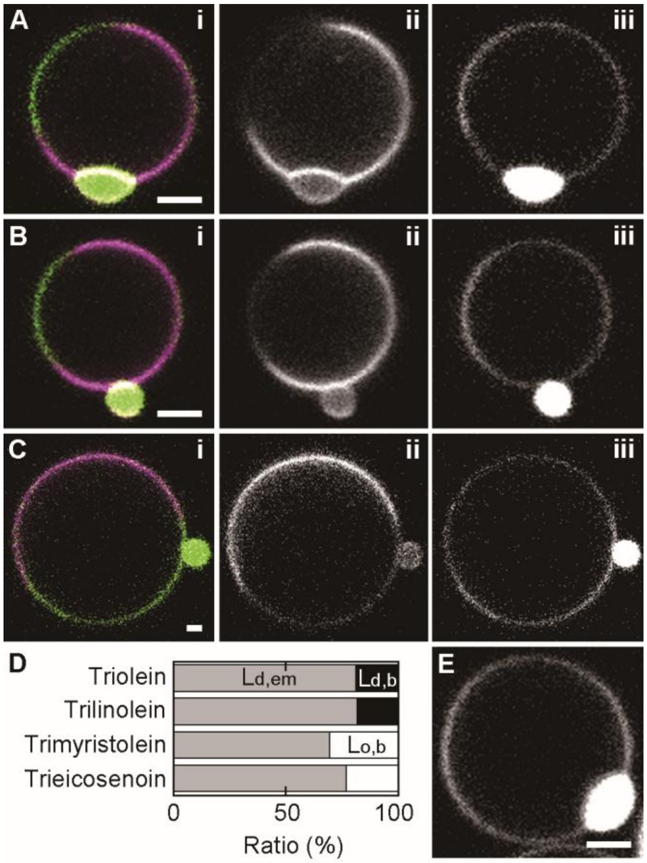

FIGURE 3. Confocal microscopy data of the GUVs after incubation with TAG droplets labeled with TopFluor-TG. Fluorescence images of the DOPC/DPPC/cholesterol (3:3:2) GUVs labeled with TR-DHPE and NBD-DPPE incorporating (A) and (B) triolein droplets and (C) trimyristolein droplets. (i) Dual-color images of the TR (magenta) and NBD/TopFluor fluorescence signals (green) and the component images of the (ii) TR and (iii) NBD/TopFluor dyes. (D) Ratios of the number of droplets incorporated in the inter-leaflet space in the L_d-phase bilayer ($L_{d,em}$, gray bar), as in (A), number of droplets bound to the outer vesicle surface in the L_d phase ($L_{d,b}$, black bar), as in (B), and number of droplets bound to the outer vesicle surface in the L_o phase ($L_{o,b}$, white bar), as in (C). The total number of the droplets analyzed for each TAG species was 11–42. (E) NBD and TopFluor fluorescence image of a DOPC/DPPC/cholesterol (1:12:7) GUV labeled with NBD-DPPE obtained after incubation with triolein droplets. The scale bars are 2 μm.

Surface Pressure Measurements of the Triolein-Containing Monolayers at the Air–Water Interface. To identify the factors that determine the distribution of TAG droplets, we now consider a droplet in the L_d-phase bilayer (Figure 4A) and a droplet in the L_o-phase bilayer with the same drop shape (Figure 4B). Each droplet is enclosed by monolayers 1 and 2, which merge into a bilayer around the droplet. The free energy difference (ΔG) between the two droplets is given by[46, 47]

$$\Delta G = \left(\gamma_{1,d} - \gamma_{1,o}\right)A_1 + \left(\gamma_{2,d} - \gamma_{2,o}\right)A_2 + (\tau_d - \tau_o)L, \quad (1)$$

where $\gamma_{i,j}$ ($i = 1, 2; j = \mathrm{d, o}$) is the interfacial tension at the TAG–water interface with monolayer i linked to the L_j-phase bilayer, A_i is the droplet surface area covered with monolayer i, τ_j is the line tension along the boundary where monolayer 1, monolayer 2, and the L_j-phase bilayer join, and L is the length of the monolayer–bilayer junction. Equation 1 shows that the droplet distribution in the two phases is determined by the first two interfacial-tension terms and the last line-tension term. However, for micrometer-sized droplets, the line-tension term is probably insignificant because of the relatively large contribution from the interfacial tension. Previous studies have shown that in comparison with τ_j, which is on the order of 1–10 pN,[6, 46, 47] the contributions from $\gamma_{i,j}$ are relatively large (~1 mN/m).[6, 46] Thus, the droplet sorting in the L_d phase appears to result from the interfacial-tension contribution. To verify this interpretation, we investigated the interfacial tension.

We previously found that the interfacial tension of monolayer-covered TAG–water interfaces can be determined from the surface pressure of the TAG-containing monolayers at the air–water interface.[48] Therefore, we first investigated the surface pressure of the triolein-containing monolayers at the air–water interface using a Langmuir trough (Figure 5). The surface pressure–

area isotherms of the DPPC/triolein monolayers showed inflection points (Figure 5A, arrows). As the area per DPPC molecule decreased below the values at these points, the surface pressure curves with different triolein concentrations overlapped. Based on previous studies of egg phosphatidylcholine (PC)/triolein[40] and 1-palmitoyl-2-oleoyl-*sn*-glycero-3-phosphocholine/tricaprylin monolayers,[48] we attributed the inflection points to the transition points at which triolein molecules began to be expelled from the DPPC monolayers to create a new bulk phase on the monolayers. The data at 20% triolein (Figure 5A, blue) exhibited another inflection point (the blue asterisk in the insert) before triolein removal from the monolayer occurred. When the triolein concentration was decreased to 10% (Figure 5A, red), this inflection point (the red asterisk in the insert) was closer to the phase transition point of a pure DPPC monolayer from a liquid-expanded state to a condensed state (the black asterisk).[49] Therefore, we assumed that a condensed phase consisting of DPPC began to form at the additional inflection points.

To verify this assumption, we conducted AFM imaging of a DPPC/triolein (4:1) monolayer which was transferred onto a mica surface with a surface pressure of 35 mN/m. The AFM data (Figure 6A and B) showed the presence of two types of domains with different heights (~0.6 nm difference). Considering the thickness of the DPPC headgroup (~0.8 nm),[50] the thick and thin domains were assigned to a condensed phase consisting of DPPC and a fluid phase mainly consisting of triolein, respectively (Figure 6C).

The condensation of the monolayers occurred because of the high chain-melting temperature of DPPC (41 °C).[37] In contrast, DOPC, which has a low melting temperature (−18 °C),[51] will create a homogeneous monolayer with triolein, as shown in Figure 6D. Consistent with this notion, the surface pressure–area isotherms of the DOPC/triolein monolayers only showed a single inflection point (Figure 5B, arrows). These points are likely to be the points at which triolein removal from the monolayers occurred.

The DPPC/triolein and DOPC/triolein monolayers were stable during lateral compression. However, the cholesterol/triolein films were unstable (Figure 5C). The surface pressure curves had an inflection point, which was apparently generated owing to triolein removal from the monolayer. However, after these points, the data at different triolein concentrations did not overlap. Additionally, in the area per lipid region of <40Å^2, the triolein-containing monolayers had smaller surface pressures than that of the pure cholesterol monolayer. These results suggest that the number of interfacial cholesterol molecules decreased owing to cholesterol solubilization in the triolein bulk phase. Cholesterol is more soluble in triolein than PCs. The solubilities of cholesterol and egg PC in triolein have been previously determined to be ~3 and <1 wt. %, respectively.[52, 53] Because of the monolayer instability, we were unable to determine the surface pressure for the cholesterol/triolein monolayers.

We also measured the surface pressure of the triolein monolayers (Figure 5D). The surface pressure increased to 13.7 (±0.1) mN/m ($N = 4$) by compression, and it did not significantly change by further compression. Similar behavior has been observed for triolein and tricaprylin.[40, 48, 54] According to the assignments for these monolayers, we attributed the inflection point to the point of monolayer collapse.

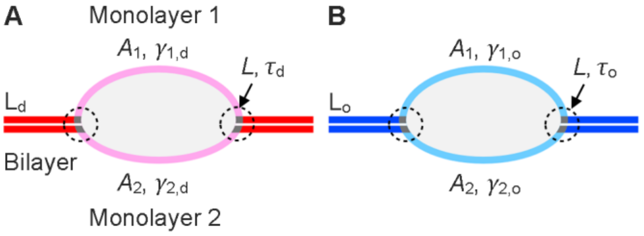

FIGURE 4. Droplets incorporated in the L_d (A) and L_o (B) phases, which are characterized by the monolayer surface area A_i, interfacial tension $\gamma_{i,j}$, length L of the boundary between the bilayer and the monolayers, and line tension τ_j along the boundary (i = 1, 2; j = d, o).

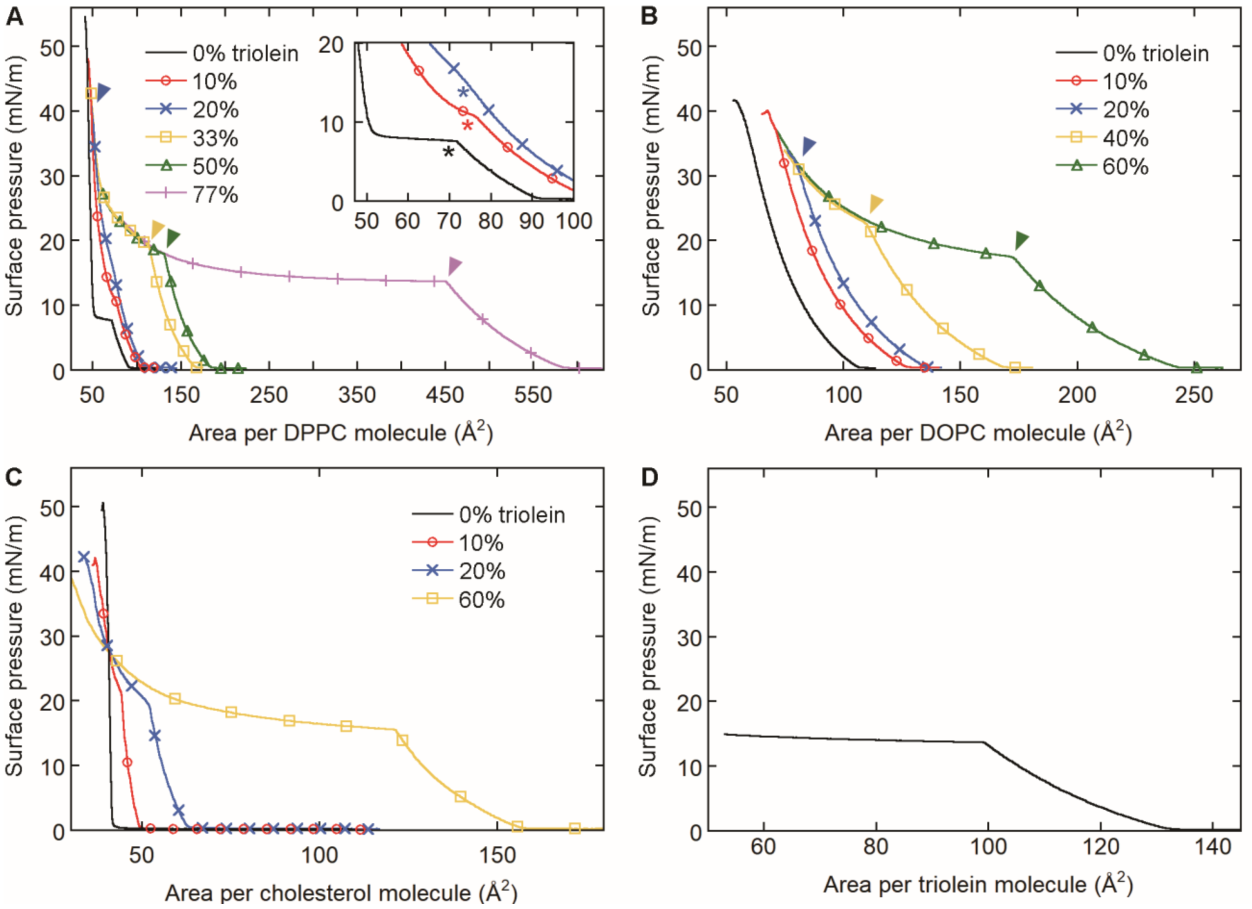

FIGURE 5. Surface pressure–area isotherms of the (A) DPPC/triolein, (B) DOPC/triolein, (C) cholesterol/triolein, and (D) triolein monolayers at the air–water interface. The arrows in (A) and (B) indicate the starting points of triolein exclusion from the monolayers. The asterisks in the insert in (A) indicate additional inflection points. The triolein ratios in the chloroform solutions spread on the subphase water are given in (A)–(C).

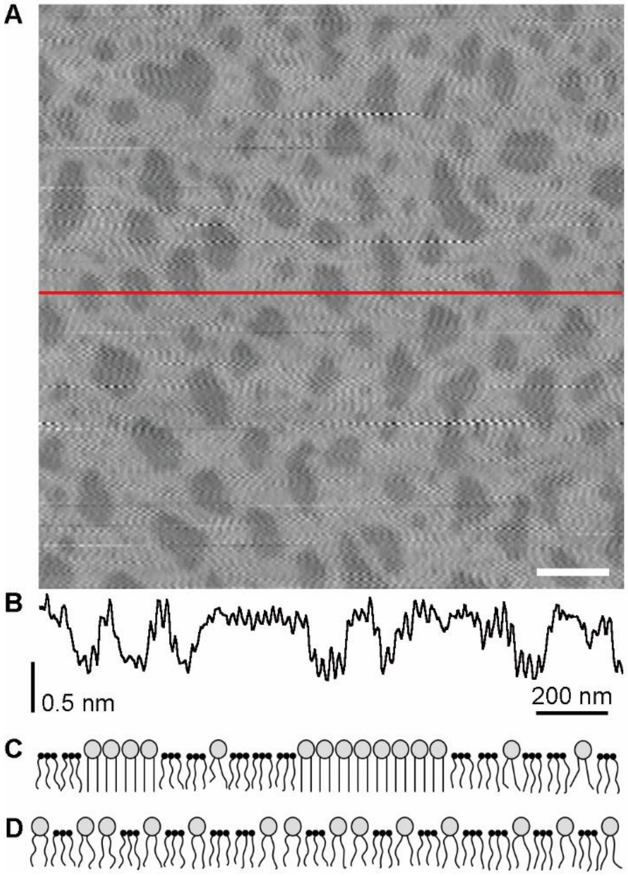

FIGURE 6. (A) AFM image of a DPPC/triolein (4:1) monolayer on a mica surface and (B) the profile along the red line in (A). The scale bar in (A) is 200 nm. Illustrations of the (C) DPPC/triolein and (D) DOPC/triolein monolayers.

Interfacial Tension at the Triolein–Water Interface. We previously found that the interfacial tension (γ) of a lipid monolayer at the TAG–water interface can be determined from surface pressure measurements using the following equation:[48]

$$\gamma = \gamma_0 + \Pi_0 - \Pi, \qquad (2)$$

where γ_0 is the interfacial tension at the pure TAG–water interface, Π_0 is the collapse pressure of the pure TAG monolayer at the air–water interface, and Π is the surface pressure of the TAG-containing monolayer at the air–water interface above the transition point from the monolayer phase to the bulk phase. Thus, we determined the interfacial tension (Figure 7) by converting the surface pressure (Figure 5), instead of directly measuring the interfacial tension. Pendant drop tensiometry is a powerful technique for determining the interfacial tension.[55] However, its drawback is that the area per lipid at the interface cannot be determined. Hence, the conversion of the surface pressure is a useful approach. The data conversion is possible because the bulk TAG molecules near the TAG–water interface have a negligible effect on the interfacial monolayer tension.[48] Using Equation 2 with the values $\gamma_0 = 30.9$ mN/m (Materials and Methods) and $\Pi_0 = 13.7$ mN/m (Figure 5D), we obtained the interfacial tension values of the DPPC and DOPC monolayers at the triolein–water interface (Figure 7A). The results revealed that at a given phospholipid surface density (Figure 7B), DOPC produced a smaller interfacial tension than DPPC. Interfacial tension data were not obtained for the cholesterol monolayer because the cholesterol/triolein monolayers at the air–water interface were unstable (Figure 5C). Nevertheless, cholesterol has a smaller polar group than PCs, and it is therefore less capable of stabilizing the TAG–water interface than PCs. Thus, at the same lipid surface density, cholesterol yields the largest interfacial tension, whereas DOPC yields the smallest interfacial tension. Therefore, the TAG–water interface is more effectively stabilized in the order of cholesterol < DPPC < DOPC. This order explains the predominant droplet partitioning in the DOPC-enriched L_d phase (Figure 3).

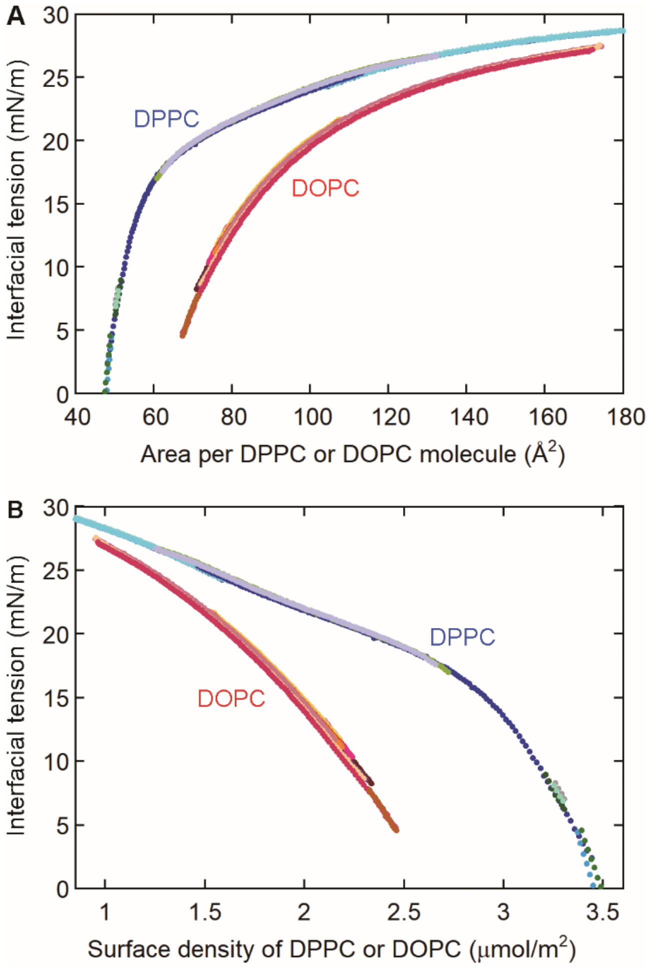

FIGURE 7. Interfacial tension data of the DPPC and DOPC monolayers at the triolein–water interface with respect to the (A) area per phospholipid molecule and (B) phospholipid surface density. The curves were drawn using one to four data obtained at each triolein percentage (10%–77% for DPPC and 10%–60% for DOPC).

Incorporation of Cholesteryl Arachidonate Droplets in GUVs. To explore the interaction between SE droplets and phase-separated bilayers, we investigated the incorporation of cholesterol arachidonate droplets labeled with BODIPY 493/503 in the DOPC/DPPC/cholesterol (3:3:2) GUVs. Fluorescence images of the GUVs in confocal imaging mode showed that the domain structures disappeared (Figure 8A). When the GUV lumen contained a droplet-free vesicle (Figure 8B), the outermost, droplet-incorporating bilayer exhibited no domain structures, whereas the bilayer of the internal vesicle was phase-separated. We also observed adsorbed vesicles in super-resolution mode with high special resolution (maximum *x*/*y* resolution 120 nm). This mode required a long imaging time (>2 s), but it was applicable to the vesicles immobilized on the glass surface. An adsorbed vesicle consisting of an outermost bilayer with droplets and an inner vesicle with no droplets (Figure 8C) showed uniform fluorescence intensity on the outer bilayer and inhomogeneous fluorescence intensity on the inner bilayer. These results indicated that phase separation at the sub-micrometer scale was precluded by cholesteryl arachidonate.

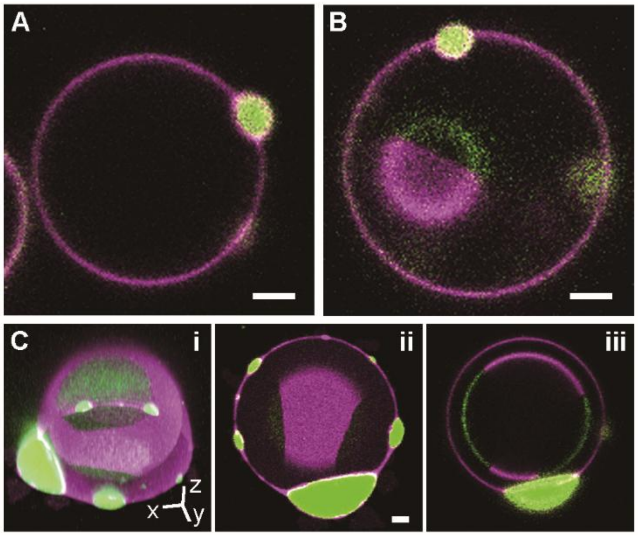

FIGURE 8. Fluorescence images obtained after the incorporation of cholesteryl arachidonate droplets labeled with BODIPY 493/503 (green) in DOPC/DPPC/cholesterol (3:3:2) GUVs with TR-DHPE (magenta) and NBD-DPPE (green). The fluorescence signals from BODIPY 493/503 and NBD-DPPE were recorded through the same acquisition channel. (A) and (B) Free vesicles visualized in confocal imaging mode. (C) Vesicle adsorbed on glass visualized in super-resolution

mode. (i) Three-dimensional image and (ii) and (iii) *x*-*y* image slices on the glass surface (ii) and 2.25 μm above the glass surface (iii). The images in (ii) and (iii) are at the same scale. The scale bars are 2 μm.

Surface Pressure Measurements of Cholesteryl-Arachidonate-Containing Monolayers at the Air–Water Interface. To further investigate the phase behavior, we measured the surface pressures of DOPC/DPPC/cholesterol (3:3:2) monolayers containing different concentrations of cholesteryl arachidonate at the air–water interface (Figure 9A). The surface pressure was plotted against the area per molecule calculated by dividing the monolayer surface area by the sum of the numbers of DOPC, DPPC, and cholesterol molecules. As monolayer compression proceeded, inflection points appeared in the curves (arrows in Figure 9A). After these points, the data overlapped. Similar behavior has been reported for PC/cholesteryl-ester monolayer systems.[56-59] These previous studies concluded that the inflection points are the transition points at which cholesteryl ester starts to move out of the monolayers. Other studies using PC monolayers and bilayers have reported that cholesteryl ester adopts a hairpin-like conformation, in which the carbonyl group in the cholesteryl ester molecule orients toward the aqueous phase and the cholesteryl residue and acyl chain extend into the hydrophobic region of the PC membrane.[58, 60] We therefore expect that the cholesteryl arachidonate molecules had hairpin-like conformations, and at the inflection points, they began to be displaced from the monolayer into the air.

The droplet-incorporating bilayers are thought to be saturated with free cholesterol arachidonate molecules, which are supplied by the droplets. Thus, the surface pressure data obtained after further compression following the inflection points are deemed to represent the state of the monolayer leaflets in the droplet-containing bilayers. Thus, we analyzed the surface pressure data to obtain information about the droplet-containing bilayers. Now consider a mixed monolayer at the air–water interface. If the component lipids are ideally mixed to form a homogeneous monolayer structure, the average area per lipid (A^{id}) at an arbitrary surface pressure is described by

$$A^{id} = \sum_i x_i A_i, \qquad (3)$$

where x_i is the mole fraction of component lipid i, and A_i is the area per lipid in a pure monolayer of component lipid i at the same surface pressure value as that of the mixed monolayer with A^{id}.[61, 62] We determined the A_i values for DOPC, DPPC, and cholesterol from the surface pressure data (Figure 5). However, the direct determination of A_i for cholesteryl arachidonate (A_{CA}) was not possible because cholesteryl arachidonate did not form monolayers at the air–water interface.[58] Therefore, assuming ideal mixing (Equation 3) and using the A_i values determined for DOPC, DPPC, and cholesterol, we calculated the A_{CA} values at the inflection points in the isotherms of the DOPC/DPPC/cholesterol (3:3:2) monolayers containing cholesteryl arachidonate (Figure 9B). The cholesteryl arachidonate molecule (Figure 1B) consists of cholesterol linked via an ester bond to arachidonic acid, which has an all-cis (20:4) acyl chain. The values of the area per lipid in the pure cholesterol monolayer at surface pressures of 15, 20, and 25 mN/m (23 °C) were determined to be 40.8 (±0.1), 40.6 (±0.1), and 40.5 (±0.1) Å^2, respectively (N = 4) (Figure 5C, black). Additionally, a previous study using stearidonic acid consisting of an all-cis (18:4) acyl chain found that the area per stearidonic acid molecule values (10 °C) at surface pressures of 15, 20, and 25 mN/m were ~51, ~46, and ~42 Å^2, respectively. Therefore, in the region of 15–25 mN/m, the sums of the area-per-molecule values for cholesterol and stearidonic acid are ~83–92 Å^2, which are similar to the calculated A_{CA} values (Figure 9B). Thus, it seems reasonable to expect that the

DOPC/DPPC/cholesterol (3:3:2) monolayers with cholesteryl arachidonate formed a nearly homogeneous structure owing to almost ideal mixing.

We also plotted the mean area per lipid at the inflection point (Figure 9A, arrows) against the cholesteryl arachidonate ratio (Figure 9C). The mean area per lipid was calculated by dividing the monolayer surface area by the number of all lipids including cholesteryl arachidonate. The data showed a linear relationship (dashed line), which was extrapolated to a mean area per lipid of 48.0 $Å^2$ at zero cholesteryl arachidonate content. This area value represents the imaginary monolayer with no cholesteryl arachidonate but the same interactions between DOPC, DPPC, and cholesterol molecules as in the presence of cholesteryl arachidonate. Because the inflection point at 5% cholesteryl arachidonate occurred at a surface pressure of ~25 mN/m (Figure 9B), this imaginary condition had to occur above ~25 mN/m. Compared with the value of 25 mN/m, the real monolayer system at 0% cholesteryl arachidonate, with a mean area per lipid of 48.0 $Å^2$ had a lower surface pressure (23.5 (±0.9) mN/m ($N = 3$), Figure 9A, black). When monolayer condensation occurs, the surface pressure–area isotherm obtained for the ideally mixed monolayer shifts toward smaller mean area per lipid. Therefore, the results suggested that cholesteryl arachidonate weakened the lipid–lipid interaction and expanded the monolayer. Thus, the surface pressure data suggested that cholesteryl arachidonate interrupted bilayer phase separation.

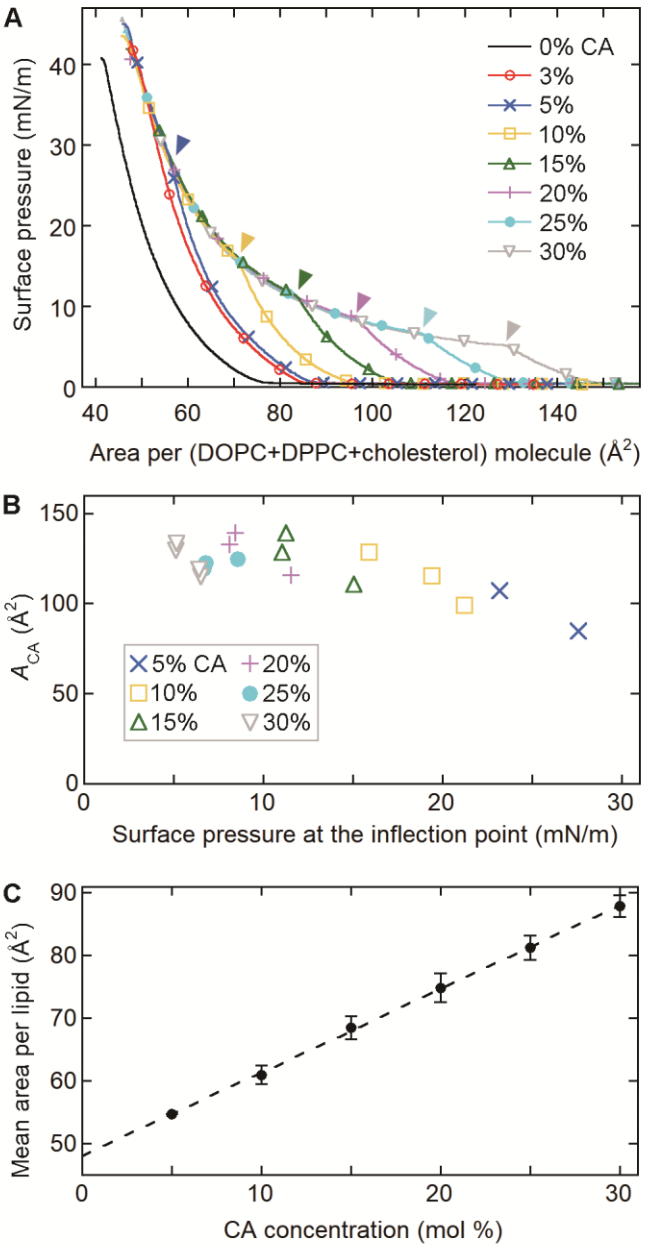

FIGURE 9. Surface pressure data of DOPC/DPPC/cholesterol (3:3:2) monolayers containing different cholesteryl arachidonate (CA) concentrations at the air–water interface. (A) Dependence of the surface pressure on the average area per lipid calculated by dividing the total monolayer surface area by the sum of the numbers of DOPC, DPPC, and cholesterol molecules. The arrows indicate the inflection points at which CA exclusion from the monolayers likely occurred. (B) Dependence of A_{CA} calculated at the inflection points (arrows in A) on the surface pressure. See

the text for the definition of A_{CA}. (C) Dependence of the mean area per lipid at the inflection point in (A) on the CA ratio. The mean area per lipid was calculated by dividing the monolayer surface area by the total number of lipid molecules. The CA ratios in the chloroform solutions spread on the subphase water are given in (A) and (B). For (B) and (C), we obtained three data at 10%, 15%, 20%, and 25% CA, four data at 30% CA, and two data at 5% CA.

Conclusions

We investigated the incorporation of TAG and SE droplets in GUVs. We found that after incorporating TAG droplets, DOPC/DPPC/cholesterol (3:3:2) GUVs retained the phase-separated state. The TAG droplets preferentially partitioned in the L_d domains. We concluded that the droplet sorting occurred because of the interfacial tension difference between the droplets incorporated in the L_d-phase bilayer and those incorporated in the L_o-phase bilayer. We also found that the bilayers incorporating cholesteryl arachidonate droplets showed no evidence for membrane phase separation in their fluorescence images and surface pressure data. The results suggested that cholesteryl arachidonate expanded the membranes and disrupted the phase separation.

ASSOCIATED CONTENT

Supporting Information. The following file is available free of charge.

Fluorescence images of the vesicles consisting of a single-bilayer region and a double-bilayer region (PDF).

AUTHOR INFORMATION

Corresponding Author

Chiho Kataoka-Hamai − Research Center for Macromolecules and Biomaterials, National Institute for Materials Science, 1-1 Namiki, Tsukuba, Ibaraki 305-0044, Japan; orcid.org/0000-0002-4068-0405; Email: kataoka.chiho@nims.go.jp

Authors

Jingwen Song − Research Center for Macromolecules and Biomaterials, National Institute for Materials Science, 1-1 Namiki, Tsukuba, Ibaraki 305-0044, Japan; orcid.org/0000-0003-1910-9287

Kohsaku Kawakami − Research Center for Macromolecules and Biomaterials, National Institute for Materials Science, 1-1 Namiki, Tsukuba, Ibaraki 305-0044, Japan; Graduate School of Pure and Applied Sciences, University of Tsukuba, 1-1-1 Tennodai, Tsukuba, Ibaraki 305-8577, Japan; orcid.org/0000-0002-3466-9365

Notes

The authors declare no competing financial interest.

ACKNOWLEDGMENTS

This work was supported by a KAKENHI grant (22K05179) from the Japan Society for the Promotion of Science. We thank Edanz (https://jp.edanz.com/ac) for editing a draft of this manuscript.

REFERENCES

(1) Olzmann, J. A.; Carvalho, P. Dynamics and Functions of Lipid Droplets. *Nat. Rev. Mol. Cell Biol.* **2019**, *20*, 137–155.
(2) Mathiowetz, A. J.; Olzmann, J. A. Lipid Droplets and Cellular Lipid Flux. *Nat. Cell Biol.* **2024**, *26*, 331–345.
(3) Farese, J., R. V.; Walther, T. C. Glycerolipid Synthesis and Lipid Droplet Formation in the Endoplasmic Reticulum. *Cold Spring Harb. Perspect. Biol.* **2023**, *15*, a041246.
(4) Chung, J.; Wu, X. D.; Lambert, T. J.; Lai, Z. W.; Walther, T. C.; Farese, J., R. V. LDAF1 and Seipin Form a Lipid Droplet Assembly Complex. *Dev. Cell* **2019**, *51*, 551–563.
(5) Arlt, H.; Sui, X. W.; Folger, B.; Adams, C.; Chen, X.; Remme, R.; Hamprecht, F. A.; DiMaio, F.; Liao, M. F.; Goodman, J. M.; et al. Seipin Forms a Flexible Cage at Lipid Droplet Formation Sites. *Nat. Struct. Mol. Biol.* **2022**, *29*, 194–202.
(6) Chorlay, A.; Thiam, A. R. An Asymmetry in Monolayer Tension Regulates Lipid Droplet Budding Direction. *Biophys. J.* **2018**, *114*, 631–640.
(7) Kataoka-Hamai, C. Triacylglycerol-Droplet-Induced Bilayer Spontaneous Curvature in Giant Unilamellar Vesicles. *Biophys. J.* **2024**, *123*, 1857–1868.
(8) Santinho, A.; Salo, V. T.; Chorlay, A.; Li, S. Q.; Zhou, X.; Omrane, M.; Ikonen, E.; Thiam, A. R. Membrane Curvature Catalyzes Lipid Droplet Assembly. *Curr. Biol.* **2020**, *30*, 2481–2494.
(9) Kataoka-Hamai, C.; Kawakami, K. Ostwald Ripening of Triacylglycerol Droplets Embedded in Glass-Supported Phospholipid Bilayers. *Langmuir* **2023**, *39*, 10001–10010.
(10) Salo, V. T.; Li, S. Q.; Vihinen, H.; Hölttä-Vuori, M.; Szkalisity, A.; Horvath, P.; Belevich, I.; Peränen, J.; Thiele, C.; Somerharju, P.; et al. Seipin Facilitates Triglyceride Flow to Lipid Droplet and Counteracts Droplet Ripening via Endoplasmic Reticulum Contact. *Dev. Cell* **2019**, *50*, 478–493.
(11) Hegaard, F. V.; Klenow, M. B.; Simonsen, A. C. Lens Nucleation and Droplet Budding in a Membrane Model for Lipid Droplet Biogenesis. *Langmuir* **2022**, *38*, 9247–9256.
(12) Puza, S.; Caesar, S.; Poojari, C.; Jung, M.; Seemann, R.; Hub, J. S.; Schrul, B.; Fleury, J. B. Lipid Droplets Embedded in a Model Cell Membrane Create a Phospholipid Diffusion Barrier. *Small* **2022**, *18*, 2106524.
(13) Caillon, L.; Nieto, V.; Gehan, P.; Omrane, M.; Rodriguez, N.; Monticelli, L.; Thiam, A. R. Triacylglycerols Sequester Monotopic Membrane Proteins to Lipid Droplets. *Nat. Commun.* **2020**, *11*, 3944.
(14) Maxfield, F. R.; Tabas, I. Role of Cholesterol and Lipid Organization in Disease. *Nature* **2005**, *438*, 612–621.
(15) van Meer, G.; Voelker, D. R.; Feigenson, G. W. Membrane Lipids: Where They Are and How They Behave. *Nat. Rev. Mol. Cell Biol.* **2008**, *9*, 112–124.
(16) King, C.; Sengupta, P.; Seo, A. Y.; Lippincott-Schwartz, J. ER Membranes Exhibit Phase Behavior at Sites of Organelle Contact. *Proc. Natl. Acad. Sci. U.S.A.* **2020**, *117*, 7225–7235.
(17) Shen, Y. H.; Zhao, Z. L.; Zhang, L. Y.; Shi, L. Y.; Shahriar, S.; Chan, R. B.; Di Paolo, G.; Min, W. Metabolic Activity Induces Membrane Phase Separation in Endoplasmic Reticulum. *Proc. Natl. Acad. Sci. U.S.A.* **2017**, *114*, 13394–13399.
(18) Tian, M. G.; Sun, Y. R.; Kong, X. Q.; Dong, B. L. Revealing the Phase Separation in ER Membranes of Living Cells and Tissues by NIR Ratiometric Imaging. *Anal. Chem.* **2022**, *94*, 2844–2854.
(19) Bernchou, U.; Midtiby, H.; Ipsen, J. H.; Simonsen, A. C. Correlation Between the Ripple Phase and Stripe Domains in Membranes. *Biochim. Biophys. Acta, Biomembr.* **2011**, *1808*, 2849–2858.

(20) Chen, D.; Santore, M. M. Three Dimensional (Temperature–Tension–Composition) Phase Map of Mixed DOPC–DPPC Vesicles: Two Solid Phases and a Fluid Phase Coexist on Three Intersecting Planes. *Biochim. Biophys. Acta, Biomembr.* **2014**, *1838*, 2788–2797.
(21) Li, L.; Cheng, J. X. Coexisting Stripe- and Patch-Shaped Domains in Giant Unilamellar Vesicles. *Biochemistry* **2006**, *45*, 11819–11826.
(22) Juhasz, J.; Davis, J. H.; Sharom, F. J. Fluorescent Probe Partitioning in GUVs of Binary Phospholipid Mixtures: Implications for Interpreting Phase Behavior. *Biochim. Biophys. Acta, Biomembr.* **2012**, *1818*, 19–26.
(23) Schmidt, M. L.; Ziani, L.; Boudreau, M.; Davis, J. H. Phase Equilibria in DOPC/DPPC: Conversion from Gel to Subgel in Two Component Mixtures. *J. Chem. Phys.* **2009**, *131*.
(24) Marsh, D. Liquid-Ordered Phases Induced by Cholesterol: A Compendium of Binary Phase Diagrams. *Biochim. Biophys. Acta, Biomembr.* **2010**, *1798*, 688–699.
(25) Veatch, S. L.; Polozov, I. V.; Gawrisch, K.; Keller, S. L. Liquid Domains in Vesicles Investigated by NMR and Fluorescence Microscopy. *Biophys. J.* **2004**, *86*, 2910–2922.
(26) Horn, P. J.; Ledbetter, N. R.; James, C. N.; Hoffman, W. D.; Case, C. R.; Verbeck, G. F.; Chapman, K. D. Visualization of Lipid Droplet Composition by Direct Organelle Mass Spectrometry. *J. Biol. Chem.* **2011**, *286*, 3298–3306.
(27) Testerink, N.; Ajat, M.; Houweling, M.; Brouwers, J. F.; Pully, V. V.; van Manen, H. J.; Otto, C.; Helms, J. B.; Vaandrager, A. B. Replacement of Retinyl Esters by Polyunsaturated Triacylglycerol Species in Lipid Droplets of Hepatic Stellate Cells during Activation. *Plos One* **2012**, *7*, e34945.
(28) Zhao, Y. Y.; Chen, Z.; Wu, Y.; Tsukui, T.; Ma, X. X.; Zhang, X. R.; Chiba, H.; Hui, S. P. Separating and Profiling Phosphatidylcholines and Triglycerides from Single Cellular Lipid Droplet by In-Tip Solvent Microextraction Mass Spectrometry. *Anal. Chem.* **2019**, *91*, 4466–4471.
(29) Small, D. M. The Physical State of Lipids of Biological Importance: Cholesteryl Esters, Cholesterol, Triglyceride. In *Surface Chemistry of Biological Systems*, Blank, M. Ed.; Advances in Experimental Medicine and Biology, Plenum Press, New York, 1970; pp 55–83.
(30) Cheng, B. L.; Kowal, J.; Abraham, S. Analysis of Adrenal Cholesteryl Esters by Reversed Phase High Performance Liquid Chromatography. *J. Lipid Res.* **1994**, *35*, 1115–1121.
(31) Talbott, H. A.; Plewes, M. R.; Krause, C.; Hou, X. Y.; Zhang, P.; Rizzo, W. B.; Wood, J. R.; Cupp, A. S.; Davis, J. S. Formation and Characterization of Lipid Droplets of the Bovine Corpus Luteum. *Sci. Rep.* **2020**, *10*, 11287.
(32) Thiam, A. R.; Ikonen, E. Lipid Droplet Nucleation. *Trends Cell Biol.* **2021**, *31*, 108–118.
(33) Chen, P. S.; Toribara, T. Y.; Warner, H. Microdetermination of Phosphorus. *Anal. Chem.* **1956**, *28*, 1756–1758.
(34) Angelova, M. I.; Soléau, S.; Méléard, P.; Faucon, J. F.; Bothorel, P. Preparation of Giant Vesicles by External AC Electric Fields. Kinetics and Applications. In *Trends in Colloid and Interface Science VI, Progress in Colloid & Polymer Science*, Helm, C., Lösche, M., Möhwald, H. Eds.; Vol. 89; Steinkopff, 1992; pp 127–131.
(35) Kataoka-Hamai, C.; Kawakami, K. Domain Sorting in Giant Unilamellar Vesicles Adsorbed on Glass. *Langmuir* **2021**, *37*, 1082–1088.
(36) Witkowska, A.; Jablonski, L.; Jahn, R. A Convenient Protocol for Generating Giant Unilamellar Vesicles Containing SNARE Proteins Using Electroformation. *Sci. Rep.* **2018**, *8*, 9422.

(37) Almeida, P. F.; Carter, F. E.; Kilgour, K. M.; Raymonda, M. H.; Tejada, E. Heat Capacity of DPPC/Cholesterol Mixtures: Comparison of Single Bilayers with Multibilayers and Simulations. *Langmuir* **2018**, *34*, 9798–9809.

(38) *CRC Handbook of Chemistry and Physics, 84th Edition*; CRC Press, LLC, 2003.

(39) Sum, A. K.; Biddy, M. J.; de Pablo, J. J.; Tupy, M. J. Predictive Molecular Model for the Thermodynamic and Transport Properties of Triacylglycerols. *J. Phys. Chem. B* **2003**, *107*, 14443–14451.

(40) Mitsche, M. A.; Wang, L. B.; Small, D. M. Adsorption of Egg Phosphatidylcholine to an Air/Water and Triolein/Water Bubble Interface: Use of the 2-Dimensional Phase Rule To Estimate the Surface Composition of a Phospholipid/Triolein/Water Surface as a Function of Surface Pressure. *J. Phys. Chem. B* **2010**, *114*, 3276–3284.

(41) Wang, L.; Walsh, M. T.; Small, D. M. Apolipoprotein B is Conformationally Flexible But Anchored at a Triolein/Water Interface: A Possible Model for Lipoprotein Surfaces. *Proc. Natl. Acad. Sci. U.S.A.* **2006**, *103*, 6871–6876.

(42) Juhasz, J.; Sharom, F. J.; Davis, J. H. Quantitative Characterization of Coexisting Phases in DOPC/DPPC/Cholesterol Mixtures: Comparing Confocal Fluorescence Microscopy and Deuterium Magnetic Resonance. *Biochim. Biophys. Acta, Biomembr.* **2009**, *1788*, 2541–32552.

(43) Veatch, S. L.; Leung, S. S. W.; Hancock, R. E. W.; Thewalt, J. L. Fluorescent Probes Alter Miscibility Phase Boundaries in Ternary Vesicles. *J. Phys. Chem. B* **2007**, *111*, 502–504.

(44) Veatch, S. L.; Keller, S. L. Organization in Lipid Membranes Containing Cholesterol. *Phys. Rev. Lett.* **2002**, *89*, 268101.

(45) Dietrich, C.; Bagatolli, L. A.; Volovyk, Z. N.; Thompson, N. L.; Levi, M.; Jacobson, K.; Gratton, E. Lipid Rafts Reconstituted in Model Membranes. *Biophys. J.* **2001**, *80*, 1417–1428.

(46) Chorlay, A.; Forêt, L.; Thiam, A. R. Origin of Gradients in Lipid Density and Surface Tension Between Connected Lipid Droplet and Bilayer. *Biophys. J.* **2021**, *120*, 5491-5503.

(47) Deslandes, F.; Thiam, A. R.; Forêt, L. Lipid Droplets Can Spontaneously Bud Off from a Symmetric Bilayer. *Biophys. J.* **2017**, *113*, 15-18.

(48) Kataoka-Hamai, C.; Kawakami, K. Determining the Dependence of Interfacial Tension on Molecular Area for Phospholipid Monolayers Formed at Silicone Oil–Water and Tricaprylin–Water Interfaces by Vesicle Fusion. *Langmuir* **2021**, *37*, 7527–7535.

(49) Barnes, G. T., Gentle, I. R. Biological Interfaces. In *Interfacial Science: An Introduction*, 2nd ed.; Oxford University Press, 2011; pp 289–319.

(50) Vacklin, H. P.; Tiberg, F.; Fragneto, G.; Thomas, R. K. Composition of Supported Model Membranes Determined by Neutron Reflection. *Langmuir* **2005**, *21*, 2827–2837.

(51) Webb, M. S.; Hui, S. W.; Steponkus, P. L. Dehydration-Induced Lamellar-to-Hexagonal-II Phase Transitions in DOPE/DOPC Mixtures. *Biochim. Biophys. Acta* **1993**, *1145*, 93–104.

(52) Ekman, S.; Lundberg, B. Phase Equilibria and Phase Properties in Systems Containing Lecithins, Triglycerides, and Water. *Acta Chem. Scand., Ser. B* **1978**, *32*, 197–202.

(53) Jandacek, R. J.; Webb, M. R.; Mattson, F. H. Effect of an Aqueous Phase on the Solubility of Cholesterol in an Oil Phase. *J. Lipid Res.* **1977**, *18*, 203–210.

(54) Azémard, C.; Fauré, M. C.; Stankic, S.; Chenot, S.; Ibrahim, H.; Laporte, L.; Fontaine, P.; Goldmann, M.; de Viguerie, L. Influence of Unsaturations on the Organization and Air Reactivity of Triglyceride Monolayers. *Langmuir* **2022**, *38*, 711–718.

(55) Berry, J. D.; Neeson, M. J.; Dagastine, R. R.; Chan, D. Y. C.; Tabor, R. F. Measurement of Surface and Interfacial Tension Using Pendant Drop Tensiometry. *J. Colloid Interface Sci.* **2015**, *454*, 226–237.

(56) Smaby, J. M.; Baumann, W. J.; Brockman, H. L. Lipid Structure and the Behavior of Cholesteryl Esters in Monolayer and Bulk Phases. *J. Lipid Res.* **1979**, *20*, 789–795.
(57) Smaby, J. M.; Brockman, H. L. Novel Surface Phase Containing Cholesteryl Esters. 2. Nonequivalence of Cholesteryl Arachidonate and Those with 18-Carbon, Cis-Unsaturated Acyl-Groups. *Biochemistry* **1981**, *20*, 724–730.
(58) Smaby, J. M.; Brockman, H. L. Thermodynamic Equation of State for Cholesteryl Esters in Surface Phases. *Biochemistry* **1984**, *23*, 3312–3317.
(59) Smaby, J. M.; Brockman, H. L. Acyl Unsaturation and Cholesteryl Ester Miscibility in Surfaces. Formation of Lecithin-Cholesteryl Ester Complexes. *J. Lipid Res.* **1987**, *28*, 1078–1087.
(60) Hamilton, J. A.; Small, D. M. Solubilization and Localization of Cholesteryl Oleate in Egg Phosphatidylcholine Vesicles. A Carbon 13 NMR Study. *J. Biol. Chem.* **1982**, *257*, 7318–7321.
(61) Hąc-Wydro, K.; Dynarowicz-Łątka, P. The Impact of Sterol Structure on the Interactions with Sphingomyelin in Mixed Langmuir Monolayers. *J. Phys. Chem. B* **2008**, *112*, 11324–11332.
(62) Dynarowicz-Łątka, P.; Kita, K. Molecular Interaction in Mixed Monolayers at the Air/Water Interface. *Adv. Colloid Interface Sci.* **1999**, *79*, 1–17.

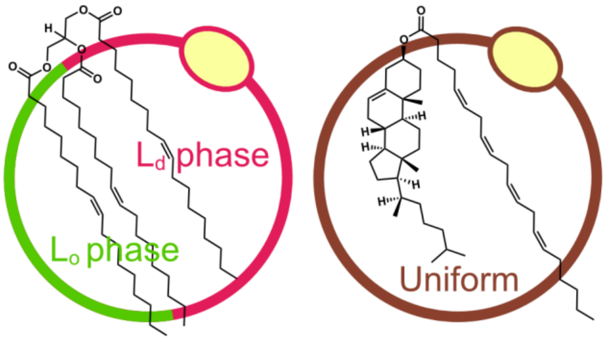

TOC graphic